LETTER

doi:10.1038/nature10740

Kimberlite ascent by assimilation-fuelled buoyancy

James K. Russell[1], Lucy A. Porritt[1], Yan Lavallée[2] & Donald B. Dingwell[2]

Kimberlite magmas have the deepest origin of all terrestrial magmas and are exclusively associated with cratons[1–3]. During ascent, they travel through about 150 kilometres of cratonic mantle lithosphere and entrain seemingly prohibitive loads (more than 25 per cent by volume) of mantle-derived xenoliths and xenocrysts (including diamond)[4,5]. Kimberlite magmas also reputedly have higher ascent rates[6–9] than other xenolith-bearing magmas[10,11]. Exsolution of dissolved volatiles (carbon dioxide and water) is thought to be essential to provide sufficient buoyancy for the rapid ascent of these dense, crystal-rich magmas. The cause and nature of such exsolution, however, remains elusive and is rarely specified[6,9]. Here we use a series of high-temperature experiments to demonstrate a mechanism for the spontaneous, efficient and continuous production of this volatile phase. This mechanism requires parental melts of kimberlite to originate as carbonatite-like melts. In transit through the mantle lithosphere, these silica-undersaturated melts assimilate mantle minerals, especially orthopyroxene, driving the melt to more silicic compositions, and causing a marked drop in carbon dioxide solubility. The solubility drop manifests itself immediately in a continuous and vigorous exsolution of a fluid phase, thereby reducing magma density, increasing buoyancy, and driving the rapid and accelerating ascent of the increasingly kimberlitic magma. Our model provides an explanation for continuous ascent of magmas laden with high volumes of dense mantle cargo, an explanation for the chemical diversity of kimberlite, and a connection between kimberlites and cratons.

Our current understanding of kimberlite ascent is greatly hampered by uncertainty about the compositions of primary kimberlite melts[1,3,5,12]. These compositions remains elusive for three reasons: kimberlites contain abundant (>30%) xenocrystic material; kimberlite melt quenched to glass has not been observed; and kimberlites are highly susceptible to alteration owing to their ultrabasic composition[1] and age[2]. Many strategies have been used to estimate kimberlite melt compositions[12,13] but the range of postulated compositions remains large and contentious (SiO_2 < 25–35%, MgO 15–25%)—especially the content of dissolved volatiles (CO_2 and H_2O)[1,3,12,13]. Physical properties estimated for the putative range of melt compositions include densities similar to basaltic or komatiitic melts (2,800–2,900 kg m^{-3}) and low viscosities (10^{-2}–10^{2} Pa s)[12].

Mantle xenoliths transported by kimberlite constrain the formation depths of these magmas to the base of the cratonic mantle lithosphere (CML) or deeper[4]. Mechanical disaggregation of xenoliths produces the mantle-olivine-dominated (>25 vol.%) suite of xenocrysts characteristic of most kimberlites (Fig. 1a). Notably, orthopyroxene (opx), which comprises ~15–27% of the CML[14–16] and is the most silicic mineral present (Fig. 1b), is rare-to-absent in kimberlite. Where observed, opx texturally records severe disequilibrium (Fig. 1c)[5,17,18]. The high crystal contents suggest bulk densities of the kimberlite magma (melt+crystal) in the range of 3.0–3.1 g cm^{-3}. Buoyant ascent of kimberlite magma from depths >120 km can be greatly enhanced by the presence of a low-density exsolved fluid phase (density of CO_2 fluid $\rho_{CO_2} \approx 1.2$ g cm^{-3} at pressure $P \approx 2$ GPa).

Here we present a mechanism for the rapid ascent of these deep-seated, high-density magmas. Our model is inspired by new

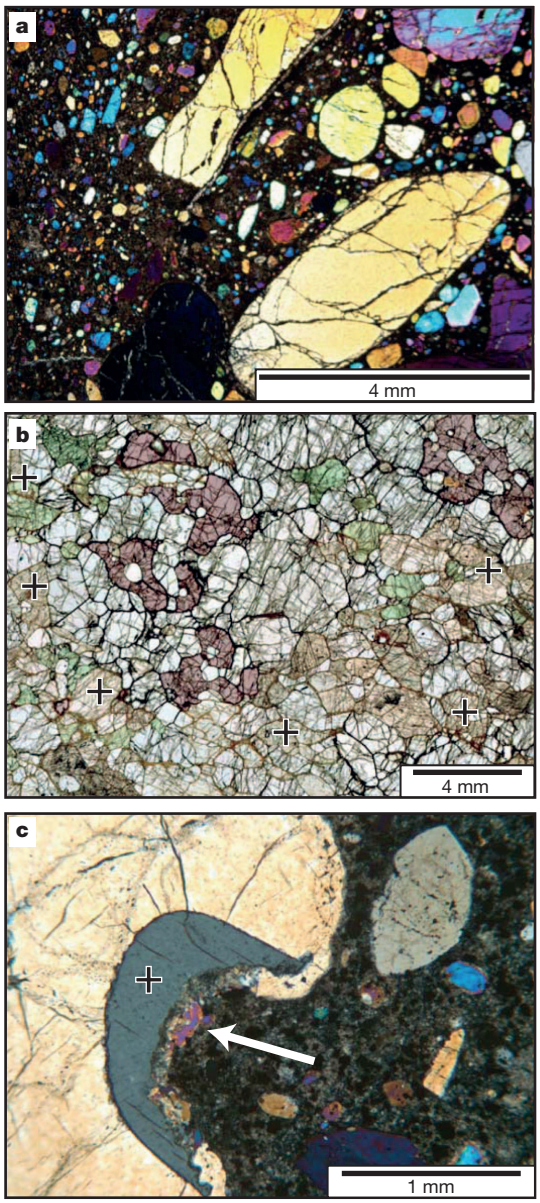

Figure 1 | Transmitted-light optical microscope images of thin sections of kimberlite, peridotite and orthopyroxene. **a**, Kimberlite hosts abundant rounded centimetre- to millimetre-scale mantle-derived xenocrysts of olivine (ol) and subordinate amounts of xenocrystic clinopyroxene (cpx), garnet (gar) and ilmenite (ilm). Orthopyroxene (opx) is conspicuously absent. **b**, Peridotitic xenolith from kimberlite, showing original mantle-equilibrated mineralogy (ol > opx > cpx > gar), textures, and grain size and shape distributions of mantle minerals. Grains of opx are marked with '+' (image courtesy of M. Kopylova). **c**, Kimberlite containing a fragment of disaggregated mantle peridotite (arrow), comprising a grain of partially dissolved opx (+; grey grain) within larger ol grain (yellow grain) (image courtesy of C. Brett).

[1]Volcanology and Petrology Laboratory, Earth and Ocean Sciences, University of British Columbia, Vancouver V6T 1Z4, Canada. [2]Department of Earth and Environmental Sciences, Ludwig Maximilian University of Munich, München 80333, Germany.

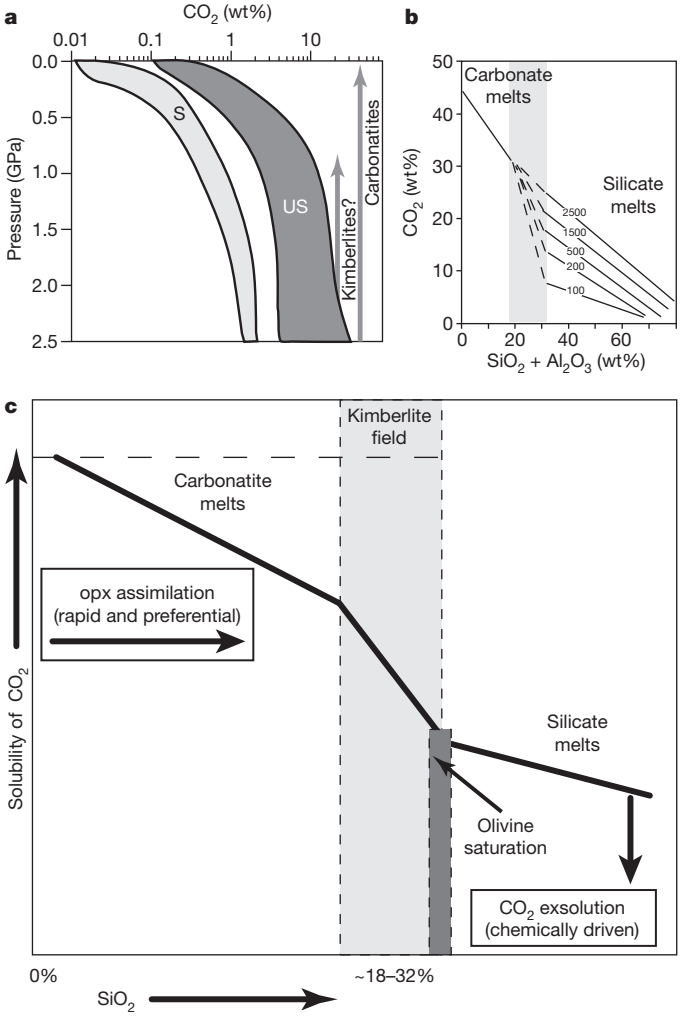

Figure 2 | CO_2 solubilities in silicic to carbonate melts (after ref. 19). **a**, CO_2 solubility limits for silica-saturated (S) and undersaturated (US) melts and hypothetical solubilities of carbonatite and kimberlite melt. **b**, Pressure and composition dependence of CO_2 solubility across the carbonate–silicate transition. Note limited effects of pressure (numbers on lines, MPa) on CO_2 solubility versus the strong effects of composition (that is, $SiO_2 + Al_2O_3$ wt%). **c**, Schematic model for assimilation-induced fluid-exsolution (that is, vesiculation) of carbonatitic or proto-kimberlitic melts. Opx assimilation drives non-silicate melts (left side) to more silicic compositions (towards right side), causing a decrease in CO_2 solubility and exsolution of a fluid phase. Continued assimilation causes continued exsolution, and results in a kimberlitic melt and olivine saturation at about 18–32 wt% SiO_2.

experimental data on the solubility of volatiles (that is, CO_2) in melts across the silicate–carbonate transition[19] (Fig. 2). This work elucidates the pressure and compositional controls on CO_2 solubility in silicic (for example, basalt to melilite) to carbonatitic melts (Fig. 2a,b) and provides three main insights. First, the solubility of CO_2 (and H_2O) in silicic melts increases with pressure but, importantly, in magmas with $SiO_2 + Al_2O_3 > 35$ wt%, solubility is limited to ~10–15%. This precludes extraordinary amounts of volatile being sequestered in parental kimberlitic melts[9,20]. Second, carbonatitic melts (that is, $SiO_2 + Al_2O_3 < 20$ wt%) have substantially higher CO_2 solubilities that are essentially independent of pressure (Fig. 2b). Solubility of CO_2 in carbonate melts is limited only by melt stoichiometry, and can be >40% (refs 21, 22). Last, the transition from carbonatitic to silicic (that is, kimberlitic) melt compositions is accompanied by a pronounced decrease in CO_2 solubility (Fig. 2b).

We suggest that melts parental to kimberlite originate as carbonatitic or near-carbonatitic melts. Such melts begin with near-stoichiometric CO_2 contents (~40 wt%) and are buoyant relative to the cratonic mantle lithosphere (density $\rho \approx 2.6$–2.8 g cm^{-3})[22]. Carbonatitic melts can also accommodate substantial amounts of water (10 wt% at 0.1 GPa) without reducing their CO_2 contents[23]. The melts entering the CML initiate the mechanical incorporation and disaggregation of xenoliths[6,24], thereby ensuring that newly liberated xenocrysts are continuously fed into the melt. At these pressures ($P < 2.5$ GPa) and temperatures ($T > 1{,}250$ °C), all mantle minerals are out of equilibrium and react with the low-a_{SiO_2} carbonatitic melt[25] (a_{SiO_2} is the activity of SiO_2). Orthopyroxene, as the most silica-saturated phase, has the highest affinity for dissolution and is assimilated rapidly and preferentially over other phases[5,17,25–27].

Assimilation of opx drives the melt towards more silicic compositions (Fig. 2c). The increased SiO_2 content of the contaminated carbonatitic melt causes a decrease in CO_2 solubility that is expressed by immediate fluid exsolution deep within the CML. Continued opx assimilation is attended by continuous fluid exsolution, leading to ever-increasing buoyancy. The process is gradual until opx assimilation produces a 'kimberlitic' melt composition ($SiO_2 > 18$ wt%), which initiates a catastrophic drop in CO_2 solubility. This results in massive exsolution of a volatile phase that reduces magma density, increases buoyancy, and supports rapid and accelerating ascent.

Results from a series of high-temperature melting experiments test these inductive ideas, and illustrate the potential speed and efficiency of the process. Our experiments involve melting powdered mixtures of Na_2CO_3 and natural mantle-derived opx ($MgSiO_3$; Fig. 3a), and measuring the weight loss as a proxy for CO_2 loss. The procedures and resulting data are fully described in Methods and Supplementary Table 1.

In non-steady-state ('transient') experiments, the melt rapidly assimilates the opx, creating a more silicic melt that is oversaturated in dissolved CO_2. The melt exsolves dissolved CO_2 (that is, undergoes decarbonation), causing a weight loss proportional to the opx content (Fig. 3b). These experiments demonstrate the spontaneous nature and rapid (~20 min) rate of the assimilation and decarbonation reactions. Reaction (that is, weight loss) continues until all of the opx has dissolved, the melt has reached its maximum SiO_2 content, and the CO_2 solubility limit of the new more silicic melt is reached (Fig. 3b). Static experiments track the change in melt composition and the production of CO_2 via melt decarbonation (Fig. 3c,d). The SiO_2 and MgO contents of the hybrid melts are greater than the bulk compositions (Fig. 3a) owing to enrichment by CO_2 loss. Na_2O content shows an initial increase and then decreases owing to the combined effects of dilution (addition of opx) and enrichment (decarbonation). CO_2 decreases dramatically. The addition of ~42 wt% opx produces SiO_2-rich (~32.7 wt%) melts in which all CO_2 is lost due to decarbonation (Fig. 3d). The maximum amount of CO_2 that would be released from the magma during assimilation to fuel the ascent of kimberlite is ~25–30 wt% (Fig. 3c, d).

Primary mantle-derived carbonatitic to near-carbonatitic (that is, low-a_{SiO_2}) melts provide an appealing model for parental kimberlite magma. Carbonatite melts are accepted as a common product of partial melting of carbonated mantle sources at pressures >2.5 GPa (refs 21, 28). Recent experimental work shows that the solidus melts of carbonated peridotite at >2.5 GPa will always be CO_2 rich and SiO_2 poor as long as carbonate is stable in the mantle assemblage[21]. These experimentally produced melts contain in excess of 40% dissolved CO_2, and can even accommodate substantial dissolved H_2O (ref. 23); we suggest that the asthenospheric production of such melts marks the onset of kimberlite ascent (Fig. 4a, b). Our mechanistic model for kimberlite ascent (Fig. 4b, c) supports petrogenetic models that interpret the diversity of kimberlite bulk rock compositions as mechanical mixing of mantle olivine (70–80%) and a carbonate-rich melt[29] combined with assimilation of mantle orthopyroxene (20–30%)[30].

We modelled the chemical evolution of the ascending melt by assuming that the amount of opx assimilated is linearly related to the

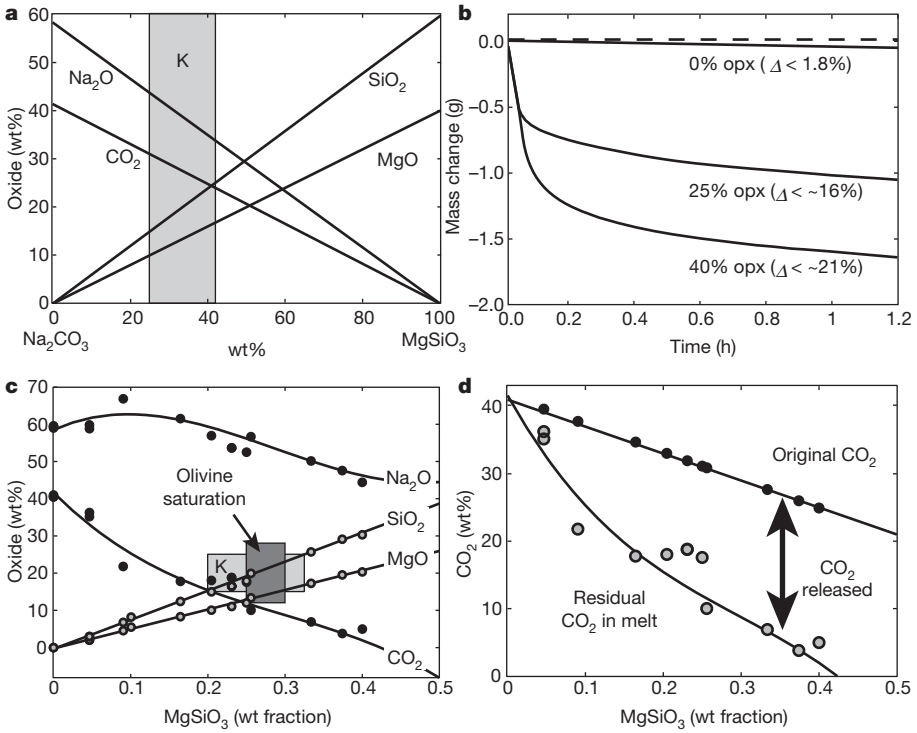

Figure 3 | High-temperature analogue experiments. **a**, Compositions produced by mechanical mixing of sodium carbonate (Na_2CO_3) and orthopyroxene (opx, $MgSiO_3$). (Data given in Supplementary Table 1). Shaded field (K) denotes range of SiO_2 contents for kimberlite melts based on Igwisi Hills kimberlite (Supplementary Table 2). **b**, Results of transient high-temperature experiments, showing mass change with time due to decarbonation driven by opx assimilation. Total weight loss (Δ) is reported in parentheses. **c**, Melt compositions produced by chemical reaction during melting of Na_2CO_3-opx mixtures versus opx content. Shaded fields mark kimberlite (K) melts and condition for olivine saturation and crystallization. **d**, Post-experiment distribution of CO_2 between hybrid melt and the exsolved fluid phase. Distance between two lines is total exsolved (released) CO_2.

distance travelled in the mantle lithosphere, and that assimilation and decarbonation are essentially instantaneous (left dashed line, Fig. 4d; Supplementary Table 2). This process can be sustained energetically by the adiabatic decompression of the magma during its ascent, which can result in considerable (150–200 °C) superheat[31]. After assimilation of ~15–20% opx, a carbonatite melt will evolve to a composition close to melt compositions estimated for the Igwisi Hills kimberlite lavas[32] (SiO_2 16–22 wt%; Supplementary Table 2; Fig. 4d). The amount of CO_2 released during assimilation and available to fuel the ascent of the contaminated carbonatite (kimberlite in the widest sense) is ~25%. Ultimately, continued opx assimilation drives the melt towards olivine saturation (Fig. 2c), allowing for late-stage magmatic crystallization of olivine as overgrowths observed on rounded olivine xenocrysts or as microphenocrysts[5,18,25,26] (Fig. 2c). Olivine crystallization would logically coincide with the later stages of kimberlite ascent and emplacement, and clearly follows on from an earlier and more extensive period of olivine disequilibrium.

The assimilation of opx is the key to this process, because it dissolves on timescales that compete with kimberlite ascent rates[25–27]. The rapid and efficient dissolution of opx, relative to other mantle xenocrysts, explains the absence of xenocrystic opx in kimberlite[5,17]. However, the main mechanistic consequence of opx assimilation is to decrease the CO_2 solubility of the melt, thereby driving deep-seated exsolution and effervescence of a CO_2-rich volatile phase (Fig. 4c). The exsolved fluid enhances the buoyancy of the ascending magma within the deep mantle, and provides an explanation for its rapid ascent and its ability to continuously entrain and transport mantle cargo to the Earth's surface.

Our model for kimberlite ascent is unique in that it begins with a low-a_{SiO_2} melt containing stoichiometric amounts of dissolved CO_2. The CO_2 is stable within the melt across a wide range of pressure–temperature conditions and, thus, exsolution of the fluid phase is not driven by depressurization, as it is in most magma ascent models. Rather, CO_2 fluid exsolution is driven by an unavoidable chemical reaction (that is, assimilation) that creates a new more silicic melt whose CO_2 solubility is exceeded; the exsolution is spontaneous and immediate. Although the initial fluid production is not driven by a change in pressure, the buoyancy of the fluid-saturated magma will be greatly enhanced by the volumetric expansion of the fluids attending depressurization. This expansion allows for continuous acceleration of the magma, entrainment of greater quantities of mantle material, and decoupling (that is, separation) of a CO_2-rich fluid phase from the ascending magma to create precursory fenitization (alkali metasomatism) events[33].

Our model provides an explanation for the linkage between kimberlites and cratons; it is clear that, if the parental magmas are carbonatitic, that a ready source of highly reactive opx is necessary to produce a more silica-rich melt (that is, kimberlite) that will exsolve fluid in the deep mantle. The cratonic mantle lithosphere has two attributes that support this transformation: first, it is enriched in opx (15–30%) relative to other mantle lithosphere[14–16]; and second, it is thick (90–120 km), and thus provides ample opportunity for sampling of opx-rich mantle. As long as the evolving carbonatitic melt is exposed to new opx, the assimilation-induced exsolution of CO_2 will continue and buoyancy is maintained or increased. Therefore, we might expect the diversity of kimberlite at the Earth's surface to actually reflect the mineralogical composition, thermal state and the thickness of the underlying mantle lithosphere rather than the source region of the melt.

The corollary is that if opx were absent, this process would not be viable, because the dissolution rates for other mantle silicates (which could also promote an assimilation-driven exsolution of fluid) are too low to keep pace with ascent rate. In addition, the enthalpy of opx dissolution is less than the heat of crystallization for olivine, implying that opx assimilation can be balanced energetically by smaller quantities of olivine crystallization and a little cooling[18]. Dissolution of olivine,

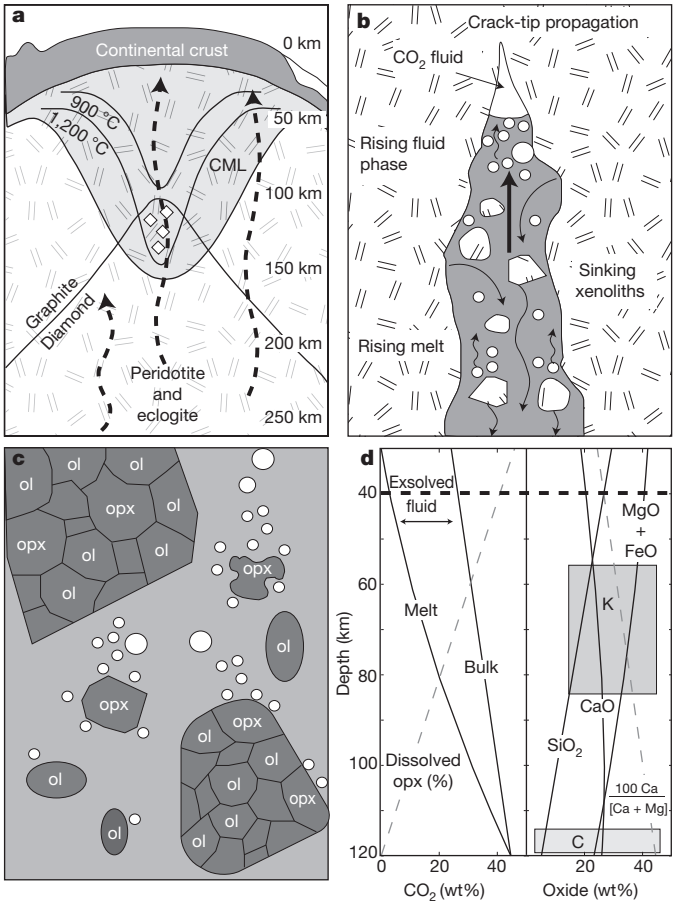

Figure 4 | Model for assimilation-fuelled ascent of kimberlite. **a**, Diverse ascent paths through cratonic mantle lithosphere (CML) shown as dashed arrows. Also shown is the line below which diamond is stable relative to graphite. **b**, Melts produced by melting of carbonated peridotite transit mantle lithosphere as dykes by crack-tip propagation, liberating dense (sinking) xenoliths to the CO_2-rich silica-undersaturated melt, and causing effervescence of buoyant (rising) CO_2-fluid. **c**, Xenoliths disaggregate and release individual mineral grains (for example, ol) to carbonatitic melt; opx grains are assimilated, preferentially promoting volatile exsolution. Deep-seated volatile production supports continued, crack-propagation-limited magma ascent. **d**, Chemical evolution of melt during ascent, including: left panel, wt% of opx assimilated (dashed line, dissolved), and CO_2 content in bulk system and in melt (solid lines); right panel, oxide (SiO_2, MgO + FeO, CaO) contents of the evolving melt (solid lines), and the 100 Ca/(Ca + Mg) ratio of melt (dashed line). Initial carbonatitic and derivative kimberlite melts (shaded boxes) defined by SiO_2 contents (Supplementary Table 2).

for example, would require substantial cooling of the magma (as well as longer times). In parts of the Earth where carbonatitic magmas do not transit the cratonic mantle lithosphere, there are only two possible outcomes. The carbonatitic melt successfully travels through a relatively thin lithosphere to be emplaced or erupted as carbonatite, or the carbonatite melt incorporates opx-poor mantle and crystallizes at depth because it fails to assimilate mantle silicates efficiently enough to promote a deep-seated fluid phase and the requisite buoyancy.

We suggest the possibility that all kimberlites start life as carbonatitic melts produced through partial melting of carbonated peridotite in the deep subcratonic mantle. As the melts transit the mantle lithosphere they continuously incorporate and disaggregate peridotite xenoliths. The low a_{SiO_2} of the carbonatitic melt causes the rapid and preferential dissolution of opx relative to the other silicate mantle minerals. This increases the silica content of the melt and triggers immediate exsolution of CO_2, reducing the buoyancy of the magma and facilitating rapid ascent. The faster the magma rises, the more mantle material will be entrained and the more opx will be dissolved. Providing opx is available, this mechanism enables the continuous and accelerating ascent of the magma and the evolution of the melt from carbonatitic to kimberlitic compositions.

METHODS SUMMARY

Our experiments use synthetic melts of Na_2CO_3 (melting temperature $T_m = 851$ °C) as an analogue for a natural carbonatitic-like melt. The experiments involve the melting of mixtures of Na_2CO_3 and crushed natural opx at temperatures of 1,000–1,100 °C for ~1 h; the mixture is open to the air. Pure Na_2CO_3 melt contains ~44 wt% dissolved CO_2 and is stable at these conditions. Melting of Na_2CO_3-opx mixtures produces vigorous decarbonation expressed by weight loss. Decarbonation results from reduced CO_2 solubility in the hybrid melt produced by opx assimilation (Fig. 2). Both transient and static experiments were performed. In the former, an initial mass of sample (Na_2CO_3 + opx) of known composition was lowered from a balance into a preheated furnace; cumulative weight loss was recorded as a function of time. The transient experiment on pure Na_2CO_3 (>1 h at 1,100 °C) shows only slight (<1.8%) change in mass and demonstrates the stability of stoichiometric amounts of CO_2 in the melt. Transient melting of Na_2CO_3-opx mixtures causes immediate reaction as opx is assimilated; the resulting hybrid melts exsolve CO_2 causing a continuous but decreasing loss in weight, until the equilibrium solubility limit of the new melt composition is reached, and weight loss ceases (<20 min). The magnitude of weight loss is taken as a quantitative measure of CO_2 loss. The tangents to the weight loss curves give the relative rates of assimilation and degassing. Static experiments saw known masses and compositions of Na_2CO_3 + opx placed into a pre-heated oven (1,000–1,100 °C) for a fixed time (Supplementary Table 1; Fig. 3a). The weight loss at the end of each experiment was measured to provide a quantitative estimate of decarbonation.

Full Methods and any associated references are available in the online version of the paper at www.nature.com/nature.

Received 29 July; accepted 28 November 2011.

1. Mitchell, R. H. *Kimberlites: Mineralogy, Geochemistry and Petrology* (Plenum, 1986).
2. Nixon, P. H. The morphology and nature of primary diamondiferous occurrences. *J. Geochem. Explor.* **53,** 41–71 (1995).
3. Kjarsgaard, B. A. in *Mineral Deposits of Canada: A Synthesis of Major Deposit-Types, District Metallogeny, The Evolution Of Geological Provinces, and Exploration Methods* (ed. Goodfellow, W. D.) 245–271 (Geological Association of Canada, Mineral Deposits Division, 2007).
4. Boyd, F. R. & Nixon, P. H. in *Lesotho Kimberlites* (ed. Nixon, P. H.) 254–268 (Lesotho National Development Corporation, Maseru, 1973).
5. Mitchell, R. H. Petrology of hypabyssal kimberlites: relevance to primary magma compositions. *J. Volcanol. Geotherm. Res.* **174,** 1–8 (2008).
6. Anderson, O. L. in *Kimberlites, Diatremes and Diamonds: Their Geology, Petrology and Geochemistry* (eds Meyer, H. O. A. & Boyd, F. R.) 344–353 (AGU, 1979).
7. Canil, D. & Fedortchouk, Y. Garnet dissolution and the emplacement of kimberlites. *Earth Planet. Sci. Lett.* **167,** 227–237 (1999).
8. Sparks, R. S. J. *et al.* Dynamical constraints on kimberlite volcanism. *J. Volcanol. Geotherm. Res.* **155,** 18 (2006).
9. Wilson, L. & Head, J. W. An integrated model of kimberlite ascent and eruption. *Nature* **447,** 53–57 (2007).
10. Sparks, R. S. J., Pinkerton, H. & Macdonald, R. The transport of xenoliths in magmas. *Earth Planet. Sci. Lett.* **35,** 234–238 (1977).
11. Spera, F. K. Carbon dioxide in petrogenesis III: role of volatiles in the ascent of alkaline magma with special reference to xenolith-bearing mafic lavas. *Contrib. Mineral. Petrol.* **88,** 217–232 (1984).
12. Sparks, R. S. J. *et al.* The nature of erupting kimberlite melts. *Lithos* **112,** 429–438 (2009).
13. Price, S. E., Russell, J. K. & Kopylova, M. G. Primitive magma from the Jericho Pipe, N.W.T., Canada: constraints on primary kimberlite melt chemistry. *J. Petrol.* **41,** 789–808 (2000).
14. Boyd, F. R. Compositional distinction between oceanic and cratonic lithosphere. *Earth Planet. Sci. Lett.* **96,** 15–26 (1989).
15. Kopylova, M. G. & Russell, J. K. Chemical stratification of cratonic lithosphere: constraints from the Northern Slave craton, Canada. *Earth Planet. Sci. Lett.* **181,** 71–87 (2000).
16. McDonough, W. F. Constraints on the composition of the continental lithospheric mantle. *Earth Planet. Sci. Lett.* **101,** 1–18 (1990).
17. Mitchell, R. H. Composition of olivine, silica activity and oxygen fugacity in kimberlite. *Lithos* **6,** 65–81 (1973).
18. Brett, R. C., Russell, J. K. & Moss, S. Origin of olivine in kimberlite: phenocryst or imposter? *Lithos* **112,** 201–212 (2009).
19. Brooker, R. A., Sparks, R. S. J., Kavanagh, J. & Field, M. The volatile content of hypabyssal kimberlite magmas: some constraints from experiments on natural rock compositions. *Bull. Volcanol.* **73,** 959–981 (2011).
20. Sparks, R. S. J., Brown, R. J., Field, M. & Gilbertson, M. A. Kimberlite ascent and eruption. *Nature* **450,** E21 (2007).
21. Dalton, J. A. & Presnall, D. C. The continuum of primary carbonatitic-kimberlitic melt compositions in equilibrium with lherzolite: data from the system CaO-MgO-Al_2O_3-SiO_2-CO_2 at 6 GPa. *J. Petrol.* **39,** 1953–1964 (1998).

22. Dobson, D. P. *et al.* In-situ measurement of viscosity and density of carbonate melts at high pressure. *Earth Planet. Sci. Lett.* **143,** 207–215 (1996).
23. Keppler, H. Water solubility in carbonatite melt. *Am. Mineral.* **88,** 1822–1824 (2003).
24. Lensky, N. G., Niebo, R. W., Holloway, J. R., Lyakhovsky, V. & Navon, O. Bubble nucleation as a trigger for xenolith entrapment in mantle melts. *Earth Planet. Sci. Lett.* **245,** 278–288 (2006).
25. Luth, R. W. The activity of silica in kimberlites: revisited. *Contrib. Mineral. Petrol.* **158,** 283–294 (2009).
26. Shaw, C. S. J. Dissolution of orthopyroxene in basanitic magma between 0.4 and 2 GPa: further implications for the origin of Si-rich alkaline glass inclusions in mantle xenoliths. *Contrib. Mineral. Petrol.* **135,** 114–132 (1999).
27. Edwards, B. R. & Russell, J. K. Time scales of magmatic processes: new insights from dynamic models for magmatic assimilation. *Geology* **26,** 1103–1106 (1998).
28. Wyllie, P. J. & Huang, W. L. Peridotite, kimberlite, and carbonatite explained in the system CaO-MgO-SiO_2-CO_2. *Geology* **3,** 621–624 (1975).
29. Canil, D. & Bellis, A. J. Phase equilibria in a volatile-free kimberlite at 0.1 MPa and the search for primary kimberlite magma. *Lithos* **105,** 111–117 (2008).
30. Patterson, M., Francis, D. & McCandless, T. Kimberlites: magmas of mixtures? *Lithos* **112,** 191–200 (2009).
31. Kavanagh, J. & Sparks, R. S. J. Temperature changes in ascending kimberlite magma. *Earth Planet. Sci. Lett.* **286,** 404–413 (2009).
32. Dawson, J. B. Quaternary kimberlitic volcanism on the Tanzania Craton. *Contrib. Mineral. Petrol.* **116,** 473–485 (1994).
33. Ferguson, J., Danchin, R. V. & Nixon, P. H. in *Lesotho Kimberlites* (ed. Nixon, P. H.) 207–213 (Lesotho National Development Corporation, Maseru, Lesotho, 1973).

Supplementary Information is linked to the online version of the paper at www.nature.com/nature.

Acknowledgements We acknowledge the laboratory support of W. Ertel-Ingritsch and S. Laumann at Ludwig Maximilian University. Funding for this research is from the Natural Sciences and Engineering Research Council (J.K.R.), a Marie Curie outbound fellowship (L.A.P.) and an ERC Advanced Researcher Grant (D.B.D.). The original manuscript benefitted from review by S. Sparks.

Author Contributions J.K.R. conceptualized the original idea, performed the static experiments at the University of Munich, and wrote the original draft paper. L.A.P. provided kimberlite expertise and context and drafted the figures. Y.L. performed the transient experiments and processed the experimental data. D.B.D. hosted, provided and repaired the experimental facility, and advised on the optimal experimental methods. All co-authors contributed to producing a final draft for review and in revising the manuscript after review.

Author Information Reprints and permissions information is available at www.nature.com/reprints. The authors declare no competing financial interests. Readers are welcome to comment on the online version of this article at www.nature.com/nature. Correspondence and requests for materials should be addressed to J.K.R. (krussell@eos.ubc.ca).

METHODS

Experiments. We have used a series of high-temperature melting experiments to illustrate aspects of the proposed model for the ascent of kimberlite. Our experiments use synthetic melts of sodium carbonate as an analogue for a natural carbonatitic melt that could be parental (that is, pre-assimilation) to kimberlites. The experimental results provide a semiquantitative test of the ideas advanced in our manuscript. The experiments (for example, conditions, melt compositions, and scales) are not intended to mimic the natural process exactly, but to illustrate what is possible and how the process may operate during magma transport.

Our experimental design follows ref. 34, in which was explored the melting reactions between superliquidus sodium carbonate (Na_2CO_3) and silica sand. Pure Na_2CO_3 melt contains ~44 wt% (50 mol%) dissolved CO_2. Fusion of the mechanical mixtures of Na_2CO_3 and silica sand at temperatures above melting ($T_m > 851\,^{\circ}C$) caused the Na_2CO_3 melt to react vigorously with the silica grains and exsolve CO_2 to the atmosphere[34].The magnitude of CO_2 loss was quantitatively expressed as a loss in weight and trivial weight loss due to Na_2O volatilization was demonstrated[34].The decarbonation of the melts continues until the SiO_2 contents of the hybrid melts exceed the stoichiometry of sodium orthosilicate ($Na_4SiO_4 \approx 32.7$ wt%) causing crystallization of the silicate phase.

Our experiments used Na_2CO_3 melts at superliquidus temperatures of 1,000–1,100 °C into which natural orthopyroxene (opx, $MgSiO_3$) had been added (Supplementary Table 1). The high superliquidus temperatures were chosen to ensure complete reaction and to suppress crystallization of new oxide or silicate minerals and are not necessarily applicable to the natural process (that is, kimberlite ascent). The opx derives from a fresh sample of cratonic mantle peridotite from the Jericho kimberlite, NWT, Canada[35]. The sample was coarsely crushed and opx grains were hand-picked under a binocular microscope; an aliquot of >150 g of orthopyroxene grains was then washed, dried and finely crushed to a coarse powder (<500 μm). We then prepared batches (15–20 g) of pre-mixed starting materials comprising precisely measured masses of oven dried Na_2CO_3 powder and coarsely powdered opx; the mass fractions of the batches covered a range of opx contents from 0 to 40 wt% (Supplementary Table 1). The preparation of large batches of starting mixtures facilitated performing replicate experiments on the same bulk compositions.

Two types of experiments were performed. First, we performed transient experiments wherein a known mass of sample (Na_2CO_3 + opx) of known composition (0, 25 and 40 wt% opx) was placed in a platinum crucible and lowered from an electronic balance into a preheated furnace. The experiments were held at the controlled furnace temperature (1,000–1,100 °C) for 1–1.5 h. Each experiment provides a record of total change in mass of the crucible plus sample as a function of time. The transient experimental set-up was also used on a pure Na_2CO_3 melt in which no opx was introduced (0% opx, Supplementary Table 1). This experiment (Fig. 3b) demonstrates the long-term stability of stoichiometric amounts of dissolved CO_2 (~40 wt%) in sodium carbonate melts. Over the course of the experiment (>1 h at 1,100 °C) there is only a slight (<1.8%) cumulative change in mass, indicating that, even though performed in air, there is little to no dissociation of the melt or degassing. This stability of the Na_2CO_3 melt is also demonstrated by the static experiments (Supplementary Table 1, see below).

In the other transient experiments, the Na_2CO_3 powder melts and begins to react immediately with the mechanically mixed-in grains of opx. The Na_2CO_3 melts assimilate the opx powder creating a more silicic melt oversaturated in dissolved CO_2. The melt is forced to exsolve (effervesce) the dissolved CO_2 (that is, decarbonation), causing a continuous loss in weight (16% and 21%; Fig. 3b). The gas exsolution reaction continues until the solubility limit of the new melt composition is reached and the loss of weight with time ceases.

Interpretation of results. The transient experiments provide two insights. First, the final weight loss is a measure of the total CO_2 lost and defines the residual CO_2 in the melt; that value represents the new equilibrium CO_2 solubility of the hybrid melt. Second, the tangent to the mass loss versus time curve is a record of the relative rates of assimilation and degassing. The slope and implied rates are high initially and then decrease exponentially as the equilibrium solubility limit for the new hybrid melt is reached. The transient experiments show the spontaneous nature and rapid rate of the assimilation and decarbonation reactions; virtually all of the loss in mass occurs in the first <20 min, after which there is little change, indicating that the assimilation-induced decarbonation process is over. The experiments rapidly converge to an equilibrium state wherein all of the opx has been dissolved, the melt has reached its maximum SiO_2 content and the CO_2 solubility has been decreased as far as possible. At this point, the melt retains the amount of CO_2 dictated by its composition; the addition of more opx would foster more reaction, more weight loss, and a new more silicic melt further depleted in CO_2.

We also performed static experiments wherein a known mass of sample (Na_2CO_3 + opx) of known composition (0, 25 and 40 wt% opx) was measured into a platinum crucible, weighed, and then placed within a pre-heated oven (1,000–1,100 °C) for a fixed time (>35–75 min) (Supplementary Table 1; Fig. 3a). The sample was then removed, cooled in a desiccator, weighed and the total weight loss determined. Most experiments were run in duplicate or triplicate and several duplicates are reported in Supplementary Table 1.

Data analysis. All hybrid melt compositions are computed assuming that all available opx dissolves into carbonate melt without crystallization to create a more siliceous melt (Supplementary Table 1). Each experiment was examined visually for signs of crystallization immediately on being removed from the furnace at the end of the experimental dwell time. In every case, the crucibles contained only a clear translucent liquid. The residual CO_2 content of the melt is also calculated assuming all mass loss is due to decarbonation (that is, Na_2O volatilization is negligible[34]) and establishes the solubility limits of the hybrid melts.

These experimental results are used to predict the chemical evolution of an idealized carbonatitic melt ascending through the mantle lithosphere and preferentially assimilating opx (Fig. 4d; Supplementary Table 2). These model calculations use the following end-member compositions and relationships. We use as the parental carbonatitic melt composition KM29 from ref. 36, a melt composition produced by melting (1,430 °C, 7 GPa) of carbonated peridotite. The opx is assumed to have a single composition equivalent to that reported in sample 25-9 of ref. 35.We have modelled the CO_2 content (in wt%) of the evolving melt (W_f) using the experimentally derived (Fig. 4d) expression:

$$W_f = W_i(1 - 2.17 w_{opx}) \quad (1)$$

where W_i is the CO_2 content (in wt%) of the idealized parental carbonatitic melt, and w_{opx} is the weight fraction of opx assimilated.

The range of melt compositions generated in this fashion are reported in Supplementary Table 2, where they are compared against the melt compositions estimated for the Igwisi Hills kimberlite[32].The Igwisi Hills compositions include two measurements on matrix-rich portions of kimberlite lava and two model compositions produced by correcting one of the lava compositions for the compositional effects of xenocrystic and phenocrystic olivine. For the purposes of comparison, Supplementary Table 2 reports the Igwisi Hills compositions on a reduced basis wherein MgO represents the sum of MgO and FeO. The best agreement between our model melt compositions resulting from progressive assimilation of opx and the Igwisi Hills kimberlite melt estimates occurs at between 15 and 20 wt% assimilation.

34. Hrma, P. Reaction between sodium carbonate and silica sand at 874°C < T 1022°C. *J. Am. Ceram. Soc.* **68,** 337–341 (1985).
35. Kopylova, M. G., Russell, J. K. & Cookenboo, H. Petrology of peridotite and pyroxenite xenoliths from the Jericho kimberlite: implications for the thermal state of the mantle beneath the Slave Craton, Northern Canada. *J. Petrol.* **40,** 79–104 (1999).
36. Dalton, J. A. & Presnall, D. C. Carbonatitic melts along solidus of model lherzolite in the system CaO–MgO–Al_2O_3–SiO_2–CO_2 from 3 to 7 GPa. *Contrib. Mineral. Petrol.* **131,** 123–135 (1998).